

Native T1 Mapping as an In Vivo Biomarker for the Identification of Higher-Grade Renal Cell Carcinoma

Correlation With Histopathological Findings

Lisa C. Adams, MD,* Bernhard Ralla, MD,† Philipp Jurmeister, MD,‡ Keno K. Bressem, MD,* Ute L. Fahlenkamp, MD,* Bernd Hamm, MD,* Jonas Busch, MD, PhD,† and Marcus R. Makowski, MD, PhD*

Objectives: The aims of this study were to identify higher-grade clear cell renal cell carcinoma (cRCC) with native T1 mapping and to histologically correlate the results with the collagen volume fraction.

Materials and Methods: For this institutional review board-approved, single-center prospective study, 68 consecutive patients received abdominal magnetic resonance imaging scans at 1.5 T between January 2017 and July 2018, using a Modified Look-Locker Inversion Recovery (MOLLI) sequence. Thirty patients with cRCC (20 men; mean age, 61.9 ± 13.1 years) who underwent partial or

Received for publication July 9, 2018; and accepted for publication, after revision, August 22, 2018.

Departments of *Radiology, †Urology, and ‡Pathology, Charité–Universitätsmedizin Berlin, Berlin, Germany.

Funding: M.R.M. has received grants from the Deutsche Forschungsgesellschaft (5943/31/41, SFB 1340) and German Israel Research Foundation. B.H. has received research grants for the Department of Radiology, Charité–Universitätsmedizin Berlin from the following companies: Abbott, Actelion Pharmaceuticals, Bayer Schering Pharma, Bayer Vital, BRACCO Group, Bristol-Myers Squibb, Charite Research Organisation GmbH, Deutsche Krebshilfe, Dt. Stiftung für Herzforschung, Essex Pharma, EU Programmes, Fibrex Medical Inc, Focused Ultrasound Surgery Foundation, Fraunhofer Gesellschaft, Guerbet, INC Research, InSightec Ud, IPSEN Pharma, Kendle MorphoSys AG, Lilly GmbH, Lundbeck GmbH, MeVis Medical Solutions AG, Nexus Oncology, Novartis, Parexel Clinical Research Organisation Service, Perceptive, Pfizer GmbH, Philips, Sanofi-Aventis SA, Siemens, Spectranetics GmbH, Terumo Medical Corporation, TNS Healthcare GmbH, Toshiba, UCB Pharma, Wyeth Pharma, ZukunftsFond Berlin (TSB), Amgen, AO Foundation, BARD, BBraun, Boehring Ingelheimer, Brainsgate, PPD (Clinical Research Organisation), CELLACT Pharma, Celgene, CeloNova BioSciences, Covance, DC Devices, Inc USA, Ganymed, Gilead Sciences, GlaxoSmithKline, ICON (Clinical Research Organisation), Jansen, LUX BioSciences, MedPass, Merek, Mologen, Nuvisan, Pluristem, Quintiles, Roche, Sehumaehrer GmbH (Sponsoring eines Workshops), Seattle Genetech, Symphogen, TauRx Therapeutics Ud, Accovion, AIO (Arbeitsgemeinschaft Internistische Onkologie), ASR Advanced Sleep Research, Astellas, Theradex, Galena Biopharma, Chiltern, PRAint, Inspiremd, Medronic, Respocardia, Silena Therapeutics, Spectrum Pharmaceuticals, St Jude, TEVA, Theorem, Abbvie, Aesculap, Biotronik, InventiveHealth, ISA Therapeutics, LYSARC, MSD, Novocure, Ockham Oncology, Premier-Research, Psi-cro, Tetec-ag, Winicker-Norimed, Achaogen Inc, ADIR, AstraZeneca AB, Demira Inc, Euroscreen SA, Galmed Research and Development Ltd, GETNE, Guidant Europe NV, Holaira Inc, Immunomedics Inc, Innate Pharma, Isis Pharmaceuticals Inc, Kantar Health GmbH, MedImmune Inc, Medpace Germany GmbH (CRO), Merrimack Pharmaceuticals Inc, Millienium Pharmaceuticals Inc, Orion Corporation Orion Pharma, Pharmacyclics Inc, PIQUR Therapeutics Ltd, Pulmonx International Sàrl, Servier (CRO), SGS Life Science Services (CRO), and Treshold Pharmaceuticals Inc. L.C.A. and B.R. are participants in the BIH Charité–Junior Clinician Scientist Program funded by the Charité–Universitätsmedizin Berlin and the Berlin Institute of Health. J.B. is a participant in the BIH–Twinning Grant Program funded by the Charité–Universitätsmedizin Berlin and the Berlin Institute of Health. The funding had no role in the study design, data collection and analysis, decision to publish, or preparation of the manuscript. The remaining authors declare that they have no conflicts of interest and did not receive any funds. There are no patents, products in development, or marketed products to declare.

Supplemental digital contents are available for this article. Direct URL citations appear in the printed text and are provided in the HTML and PDF versions of this article on the journal's Web site (www.investigativeradiology.com).

Correspondence to: Lisa C. Adams, MD, Department of Radiology, Charité–Universitätsmedizin Berlin, Charitéplatz 1, 10117 Berlin, Germany. E-mail: Lisa.adams@charite.de.

Copyright © 2018 Wolters Kluwer Health, Inc. All rights reserved.

ISSN: 0020-9996/19/5402-0118

DOI: 10.1097/RAD.0000000000000515

radical nephrectomy and histological grading according to the International Society of Urological Pathology (ISUP) classification and a separate healthy cohort of 30 individuals without renal malignancies or complex cysts (16 men; mean age, 59.7 ± 14.6 years) met the eligibility criteria. T1 values were quantitatively measured with region of interest measurements in T1 maps. Quantification of the collagen volume fraction was performed on histological sections (picrosirius red staining).

Results: Native T1 values were significantly lower for lower-grade cRCC (ISUP 1 and 2) compared with higher-grade cRCC (ISUP 3 and 4; $P < 0.001$). A cutoff value of 1101 milliseconds distinguished higher-grade from lower-grade tumors with a sensitivity of 100% (95% confidence interval [CI], 0.69–1.00), a specificity of 85% (95% CI, 0.62–0.97), and an accuracy of 90% (95% CI, 0.73–0.98). Native T1 values were significantly associated with the histological collagen volume fraction ($P < 0.05$). Furthermore, T1 times in the renal cortex, medulla, and tumor tissue showed an excellent interobserver agreement.

Conclusions: Native T1 mapping could represent an in vivo biomarker for the differentiation of lower- and higher-grade cRCCs, providing incremental diagnostic value beyond qualitative magnetic resonance imaging features.

Key Words: native T1 mapping, quantitative MRI, clear cell renal cell carcinoma, in vivo tumor grading, collagen volume fraction, individualized treatment options, preoperative planning

(*Invest Radiol* 2019;54: 118–128)

Clear cell renal cell carcinomas (cRCCs) are the most common renal malignancies with continuously increasing incidence.¹ The extracellular matrix (ECM) of the stroma is an important structural component in cRCC, with collagen being the most abundant ECM protein, contributing to the development and progression of cRCC.² The correlation between upregulation of collagen and tumor progression has been investigated for different types of cancer.³ A recent study on cRCC found that upregulation of collagen type IV was associated with a poorer prognosis and with increased tumor growth in vivo.⁴ Apart from tumor size, subtype, and stage, the histological tumor grade is among the most important prognostic factors for RCC patient outcome.⁵

A reliable noninvasive and preoperative prediction of tumor grade is desirable, because the prognosis of higher-grade tumors (grades 3 and 4) is significantly worse compared to lower-grade RCCs (10-year survival of 15%–46% vs 84%–89%).⁶ With recent advances in the understanding of tumor pathophysiology,⁷ active surveillance for eligible patients with localized renal masses (T1a) has been advocated.⁸ Although most T1a tumors are benign or low grade, approximately 20% are high grade with tendencies of local invasiveness.⁸ Consequently, there is an evolving role of renal mass biopsies, which, however, carry the risk procedural complications and nondiagnostic biopsies.⁹ Therefore, a reliable noninvasive imaging technique to distinguish higher-grade from lower-grade cRCCs would be helpful to improve the diagnostic accuracy of, or even decrease the need for renal mass biopsies and to assist in triaging patients to the best individual therapy.

T1 mapping is an emerging concept for quantitative tissue characterization, evaluating the longitudinal relaxation time (T1) in each image voxel and thus providing unique quantifiable and reproducible

intrinsic tissue values.¹⁰ Therefore, it can be used as a quantitative and noninvasive method for *in vivo* histology to determine biological tissue properties, possibly as a fast and contrast-free technique.¹¹ In the context of cardiovascular imaging, it has emerged as a promising noninvasive modality for characterization of the myocardial tissue, for example, quantification of myocardial fibrosis.¹²

The objective of this study was to assess quantitative T1 values of cRCC and healthy kidneys on a subject-specific basis. We hypothesized (1) that lower-grade cRCCs were associated with significantly lower native T1 values compared with higher-grade RCCs, (2) that native T1 values showed a correlation with the collagen volume fraction on histopathological sections, and (3) that cortical, medullary, and tumor T1 values would be reproducible between observers.

MATERIALS AND METHODS

Study Design and Population

This prospective study was approved by the institutional review board (EA1/412/16), and written informed consent was obtained from all participants before the examination. Between January 2017 and July 2018, 68 consecutive patients, who agreed to participate and had no contraindications to magnetic resonance imaging (MRI) or prior radiofrequency ablation, were referred to our department for abdominal MRI. Patients with preoperatively suspected cRCC based on MRI, who underwent surgery and received histological grading as the reference standard, were included as well as patients without renal malignancies, who were considered in a separate healthy cohort. Four patients were excluded, because histology revealed urothelial carcinomas ($n = 2$) or oncocytomas ($n = 2$) instead of an RCC, and 4 patients were excluded, because they received no surgery, being considered poor surgical candidates. The final cohort consisted of 60 patients, including 30 patients with diagnosis of cRCC (mean age \pm SD, 61.9 ± 13.1 years), who underwent partial or radical nephrectomy and histological examination, and 30 patients without renal malignancies or complex cysts (mean age \pm SD, 58.6 ± 15.4 years).

Imaging Protocol

Examinations were performed by using a 1.5 T clinical MR scanner (Avanto; Siemens Medical Solutions, Erlangen, Germany) with

a dedicated 16-channel body-phased array coil. The patients underwent a clinical routine image protocol of the kidneys and, in addition, received a native and respiratory gated steady-state precession readout single-shot Modified Look-Locker Inversion Recovery (MOLLI) sequences in coronal planes, adjusted to the long axis of both kidneys. Single-shot images were acquired at a train of different inversion times after an initial inversion pulse and all images were gated to the same cardiac phase. By the combination of 3 inversions with slightly shifted TI times, the relaxation curve consisted of 3 interleaved blocks, resulting in a sufficient number of points at 8 inversion times for calculation of T1 quantification within a breath-hold of 11 heart beats. Fixed parameters were an initial TI of 153 milliseconds, a T1 increment of 80 seconds, and 3 pausing heart cycles between the blocks. Refer to Table 1 for tabulated MRI parameters. T1 maps were automatically calculated on a pixel-by-pixel basis. The resulting pixel-by-pixel maps were displayed by use of a customized 12-bit lookup table, and the color map was visible immediately after data acquisition. In the color map, the signal intensity (SI) of each pixel reflects the absolute T1 value of the underlying value.

Imaging Analysis and Region of Interest Measurements

All images were analyzed on PACS workstations (Centricity Radiology; GE Healthcare), using Visage 7.1 software (Visage Imaging, Berlin, Germany). MOLLI images were assessed independently, in randomized order and in 2 different reading sessions by 2 radiologists, who were blinded to the results of the initial assessment and the identifying data. Location of the regions of interest (ROIs) was based on a solid portion approach.¹³ Circular 2-dimensional ROIs were placed within the most homogeneous and bright-appearing portion of solid tumor area on the basis of visual assessment in the postcontrast sequences and also in conjunction with T2-weighted images and were set in as large an area as possible. The respective ROI was then copied to the MOLLI sequence, using an automatic coregistration tool and by visual correlation in case of breathing artifacts. It was taken care not to include the normal renal cortex, perinephric, or sinus fat within the measured ROIs. Regions of necrosis, cystic degeneration, and hemorrhage were avoided and identified by lack of enhancement on postcontrast images (refer to the Supplementary Fig. S1, Supplemental Digital Content 1, <http://links.lww.com/RLI/A402>, for patient examples of ROI measurements).¹⁴ For comparison of cortex and medullar relaxation times between healthy and diseased kidneys, ROIs were placed in a healthy

TABLE 1. Tabulated MRI Parameters

Sequence	T1 FLASH	T2 HASTE	MOLLI*	T1 3D-FLASH*
Scan plane	Axial	Coronal	Coronal	Coronal
Voxel size, mm	$1.4 \times 1.1 \times 4.0$	$1.7 \times 1.3 \times 5.0$	$1.9 \times 1.3 \times 4.0$	$1.6 \times 1.0 \times 1.4$
No. slices	60	25	1	1
TR/TE, ms	186/4.76	800/89	912/1.16	2.88/0.98
Averages	1	1	2	1
FoV, mm	340	400	400	500
Flip angle, degrees	70	170	35	25
Matrix	320	320	320	512
Bandwidth, Hz/Px	260	422	1042	440
Fat saturation	None	None	None	Yes
Parameter map type	—	—	T1 map	—
No. inversions	—	—	3	—
MOLLI TI start, ms	—	—	153	—
MOLLI T1 increment, ms	—	—	80	—
MOLLI T1 trigger delay, ms	—	—	160	—

MOLLI indicates Modified Look-Locker Inversion Recovery; 3D, 3-dimensional; TR, repetition time; TE, echo time; HASTE, HAlf fourier Single-shot Turbo spin-Echo; FoV, field of view.

portion of the renal cortex and medulla, avoiding positioning on the boundary between cancerous and normal parenchyma.

For additional comparative assessment of semiquantitative/qualitative parameters, conventional T1 and T2 SI (with corresponding ROI sizes and location) were also determined. With regard to contrast enhancement, SI ratios ($SI_{\text{SD}_{\text{image}} \text{ noise}}$) and contrast intensity ratios ($SI_{\text{RCC}} - SI_{\text{renal cortex}}/\text{SD}_{\text{image}} \text{ noise}$) for the corticomedullary and nephrographic phases were calculated.

Calculation of Collagen Volume Fraction

All histological RCC specimens were fixed in formalin, embedded in paraffin wax, sectioned at 2 μm , and then stained with picrosirius red to visualize and determine the collagen volume fraction. Two representative magnification ($\times 50$) tiled digital images (one of a central and one of a periphery region) were acquired per patient (Zeiss LSM 710; Carl Zeiss, Germany) for quantitative analysis with the open-access software ImageJ (ImageJ 1.50i; Wayne Rasband, National Institutes of Health). Automatic thresholding was used to get the image with the best separation of collagen fibers, with the collagen volume fraction

being calculated as the percentage of the collagen area, divided by the total depicted cRCC area.

International Society of Urological Pathology Grading Features

Resected cRCCs were examined by a pathologist and classified into 4 International Society of Urological Pathology (ISUP) grades for renal carcinoma, which were established in 2012 and recommended by the WHO (World Health Organization) as replacement for the Fuhrman grading.¹⁵ The ISUP/WHO grading system is based on the evaluation of the nucleoli, with grade 4 tumors showing extreme polymorphism, rhomboid, and/or sarcomatoid morphology.¹⁵

Statistical Analysis

Data analysis was performed with "R" Statistical Software (Version 3.2.2, R Development Core Team, 2015). Variables were expressed as means \pm SDs. Initially, a power analysis was performed to determine the minimum required sample size for a 2-tier differentiation (alpha value of 0.05, beta value of 0.02, power of 0.8). Interobserver agreement

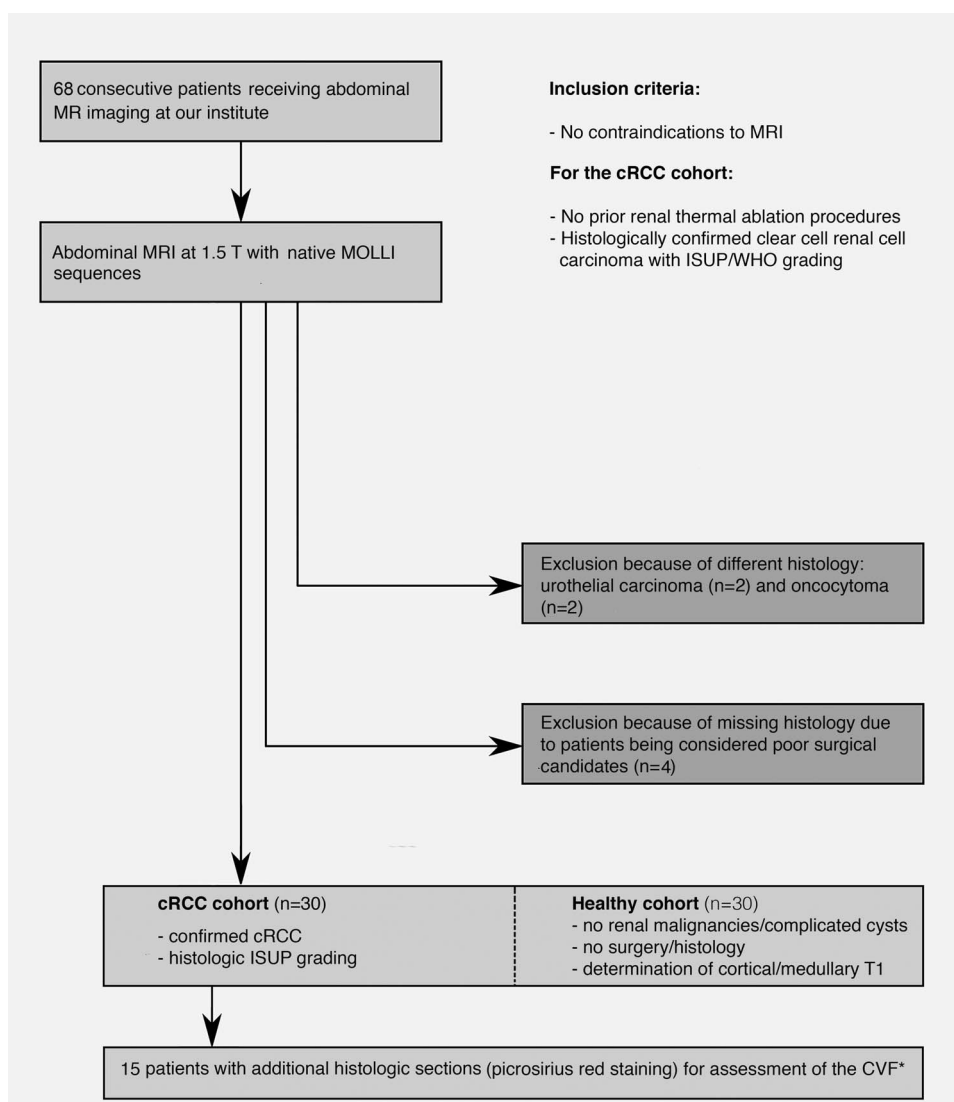


FIGURE 1. Workflow of participants through the study. This diagram illustrates the flow of study participants and shows the reasons for exclusion as well as the final study population, meeting the eligibility criteria.

between the 2 readers was assessed using the intraclass correlation coefficient (ICC) and the 95% Bland-Altman limits of agreement. An ICC value was considered to represent poor agreement, if it was below 0.40, fair agreement for values from 0.40 to 0.59, good agreement for values from 0.60 to 0.74, and excellent agreement for values above 0.75. The values obtained by the 2 observers were averaged to obtain single measurements for each region. Student *t* tests were used to assess the differences in means for continuous variables. Box plots were used for displaying the distribution of T1 values in the different groups. A receiver operating characteristic (ROC) curve analysis was performed for estimation of an optimal cutoff T1 value to identify higher-grade cRCC. As a high sensitivity is decisive for grading cRCC, sensitivity was prioritized over specificity in the exploratory selection of the optimal cutoff value to identify higher-grade cRCC. A *P* value less than 0.05 was considered statistically significant.

RESULTS

A total of 68 patients were consecutively examined, including 30 patients with cRCC and 30 patients without renal malignancies, who were considered in a separated healthy cohort (refer to Fig. 1 for workflow of participants and to Table 2 for an overview of the study characteristics). The histological grading of the 30 patients showed 8 ISUP grade 1 lesions, 12 ISUP grade 2 lesions, 5 ISUP grade 3 lesions, and 5 ISUP grade 4 lesions. There was no significant correlation

between age and ISUP grade (*P* > 0.05). The maximum cRCC diameter ranged from 1.6 cm to 13.0 cm (5.42 ± 2.97 cm), whereby—as to be expected—the size showed an increase with the grading, without reaching significance level (*P* > 0.05). Region of interest sizes for cRCC varied from 2.08 cm² to 34.20 cm² (average size 11.8 ± 10.9 cm²). For cRCC patients, the time interval between the abdominal MRI and partial or radical nephrectomy was 21.8 ± 17.4 days.

Quantitative Measurements and Analysis: Identification of Higher-Grade cRCC

Native T1 relaxation time was measured and averaged over the 2 observers. Average mean native T1 relaxation times were 925 ± 142 milliseconds for ISUP grade 1, 1070 ± 79 milliseconds for ISUP grade 2, 1191 ± 40 milliseconds for ISUP grade 3, and 1316 ± 43 milliseconds for ISUP grade 4. The differences in native T1 relaxation times between the 4 ISUP grades were highly significant, with the 2 lower grades (1 and 2) and the higher grades (3 and 4) being combined and tested against each other (*P* < 0.001; refer to Fig. 2). Higher-grade tumors (ISUP grades 3 and 4) showed significantly longer native T1 relaxation times compared with lower-grade tumors (ISUP grades 1 and 2). A ROC curve analysis was performed for determining an optimal cutoff value (Fig. 2). For a cutoff value of 1101 milliseconds to identify higher-grade tumors, sensitivity reached 100% (95% confidence interval [CI], 0.69–1.00), specificity was 85% (95% CI, 0.62–0.97), and the

TABLE 2. Characteristics of the Study Population

No. patients with cRCC (men/women)		30 (20/10)
Mean age of patients with cRCC (SD)		61.9 (13.1)
Mean glomerular filtration rate of cRCC patients		56.9 (21.3)
Partial nephrectomy (%)		50%
No. patients without cRCC (separate healthy cohort)		30 (16/14)
Mean age of patients without cRCC (SD) (men/women)		59.7 (14.6)
Grade-specific diameter range (average ± SD), cm		ISUP 1: 1.9–4.2 (4.0 ± 0.1) ISUP 2: 1.6–6.2 (4.8 ± 1.8) ISUP 3: 6.1–13 (10.8 ± 2.9) ISUP 4: 6.1–13 (9.6 ± 2.9).
Mean glomerular filtration rate of patients without cRCC		70.2 (17.7)
Average native T1 values (SD), ms		
Renal cortex		1026.8 (65.6)
Renal medulla		1254.8 (81.9)
Average T1 values for cRCC (SD, number, %), ms		
ISUP grade 1		925 (142, 8, 26.7)
ISUP grade 2		1070 (79, 11, 36.7)
ISUP grade 3		1191 (40, 6, 20)
ISUP grade 4		1316 (43, 5, 16.7)
T stage (number, number per grade)		
T1a (9)	ISUP 1	4
	ISUP 2	5
T1b (6)	ISUP 1	2
	ISUP 2	4
T2 (1)	ISUP 1	1
T3a (11)	ISUP 1	1
	ISUP 2	2
T3c (2)	ISUP 1	1
T4 (1)	ISUP 1	1
N stage (number, number per stage)		
N1 (5)	ISUP 1	3
M stage (number, number per stage)		
M1 (7)	ISUP 1	1
	ISUP 2	3
	ISUP 3	3
	ISUP 4	3

cRCC indicates clear cell renal cell carcinoma; ISUP, International Society of Urological Pathology.

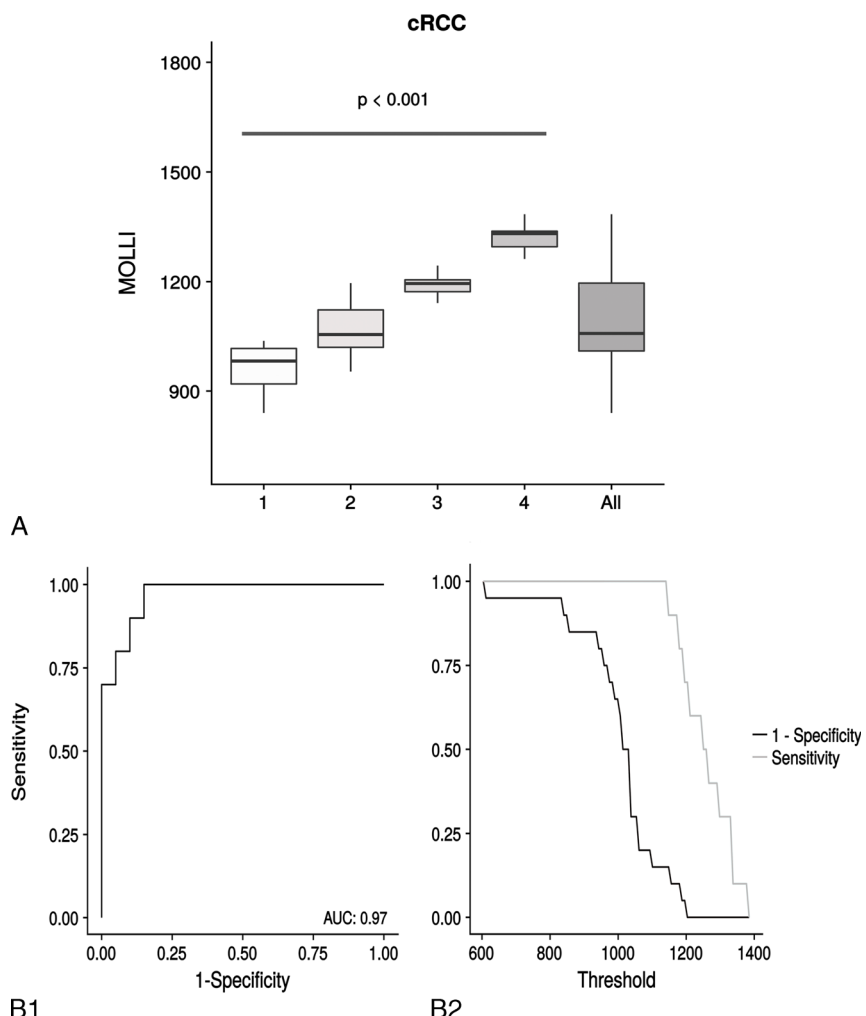


FIGURE 2. Distribution of native T1 values across the different ISUP grades in patients with cRCC. The upper part of the image (A) displays native T1 values across the different ISUP grades using box plots. The differences in native T1 relaxation times between the 2 lower grades (1 and 2) and the higher grades were significantly different ($P < 0.001$). The bottom and top of the boxes represent the first and third quartiles, the band in the box represents the median, and the ends of the whiskers indicate the minimum and maximum of all the data. The lower left part of the image (B1) illustrates the diagnostic performance of native T1 mapping as a binary classifier in discriminating between ISUP grades 1/2 and 3/4 with the T1 threshold being varied using a receiver operation characteristic curve. The corresponding area under the curve (AUC) is also provided (AUC, 0.95). The lower right part (B2) shows the sensitivity and specificity values plotted against their corresponding threshold.

accuracy was 90% (95% CI, 0.73–0.98; refer to Table 3 for confusion matrix; Fig. 2). The false-positives (low-grade tumors, showing T1 times >1101 milliseconds) were a result of the presence of cystic components (as confirmed by histology), leading to an increase in T1 times. Refer to Figure 3 for corresponding case examples of patients with cRCC (ISUP grades 1 to 4).

Semiquantitative/Qualitative Measurements: T1/T2 Signal Intensities and Contrast Enhancement

For both T1 and T2 signal intensities, we found no significant difference between lower- and higher-grade RCCs ($P > 0.05$). Although lower-grade tumors showed an averaged T1 relaxation rate of 125.5 ± 31.5 milliseconds, higher-grade cRCCs demonstrated a relaxation rate of 133.9 ± 22.9 milliseconds ($P > 0.05$). For T2 relaxation times, we measured an average of 335.5 ± 151.2 for lower-grade tumors compared with 300.7 ± 105.5 for higher-grade tumors. For SI and contrast intensity ratios for the corticomedullary and nephrographic phases, we also found no significant difference between high- and low-grade cRCCs (corticomedullary and medullary: $P > 0.05$). As a consequence,

no reliable differentiation between the grades could be made based on conventional MRI.

TABLE 3. Confusion Matrix for Calculation of Sensitivity and Specificity

MR Native T1 Mapping (Index Test)	Histology (Reference Standard)		Total
	Confirmed Higher-Grade cRCC	Confirmed Lower-Grade cRCC	
Higher-grade cRCC (ISUP grades 3 and 4)	10	3	13
Lower-grade cRCC (ISUP grades 1 and 2)	0	17	17
Total	10	20	30

MT indicates magnetic resonance; cRCC, clear cell renal cell carcinoma; ISUP, International Society of Urological Pathology.

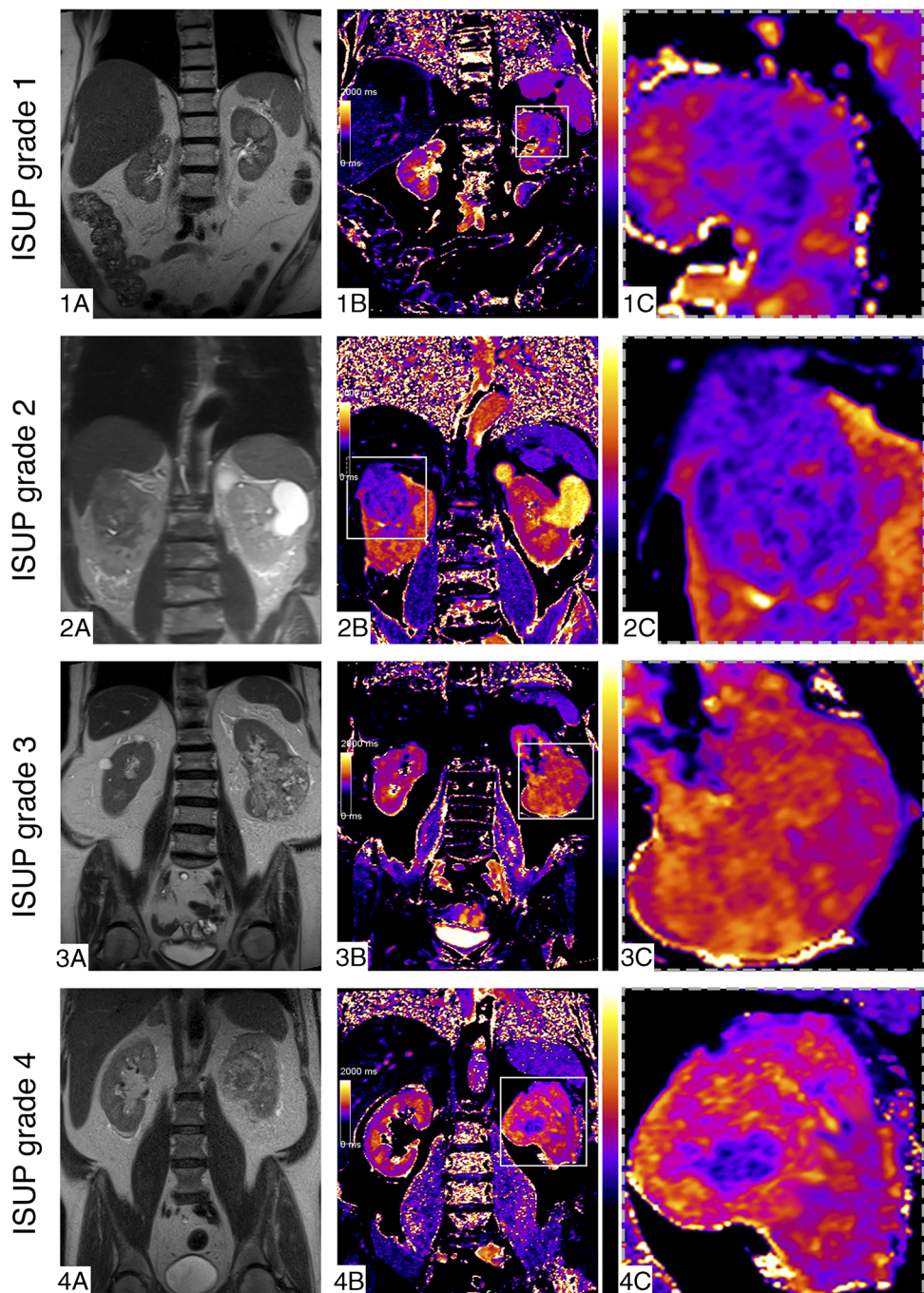


FIGURE 3. Native T1 mapping images of lower- and higher-grade cRCCs. 1A, T2 HASTE image of a 70-year-old woman with a low-grade (ISUP 1) cRCC of the left kidney. 1B, Corresponding native T1 MOLLI (Modified Look-Locker Inversion Recovery) image, showing a relatively low signal intensity, which reflects a lower T1 value. 2A, T2 HASTE image of a 56-year-old man with a lower-grade (ISUP 2) cRCC of the right kidney. 2B, Corresponding native T1 MOLLI image, also showing a relatively low signal intensity, which reflects a comparatively low T1 value. 3A, T2 HASTE image of a 76-year-old woman with a higher-grade (ISUP 3) cRCC of the left kidney. 3B, Corresponding native T1 MOLLI image, showing a relatively high signal intensity, which reflects a higher T1 value. 4A, T2 HASTE image of a 78-year-old man with a high-grade (ISUP 4) cRCC of the left kidney with central necrosis. 4B, Corresponding native T1 MOLLI image, showing a relatively high signal intensity, reflecting a high overall T1 value, with a focal low signal intensity in the center, which corresponds to the necrosis zone and was excluded from the region of interest (ROI) analysis. 1C, 2C, 3C, and 4C are magnifications of 1B, 2B, 3B, and 4B. 1A, The rectangles used in 1B, 2B, 3B, and 4B correspond to the magnified sections on the right side of the figure and were drawn for better visualization of where the magnified sections were derived from. They do not represent the ROIs chosen for analysis. HASTE, Half Fourier Single-shot Turbo spin-Echo.

Histological Collagen Volume Fraction and Its Relation to Native T1 Times

The mean histological collagen volume fraction across the different cRCC grades was $21.9\% \pm 7.5\%$. Patients with higher-grade cRCC showed significantly higher collagen volume fractions. This can also be seen in Figure 4, which illustrates histological sections stained with picrosirius red from a periphery ($\times 50$, bar, 500 μm , A) and a central ($\times 50$, bar, 100 μm , B) and part of the cRCC (refer to the Supplementary Fig. S2, Supplemental Digital Content 2, <http://links.lww.com/RLI/A403>, for better visualization of cell nuclei in sections [$\times 50$] stained with Masson Trichrome, bar, 100 μm). Native T1 values were significantly associated with the histological collagen volume fraction, showing a strong correlation ($P < 0.01$; correlation coefficient, 0.71; Fig. 5).

Association of Quantitative T1 Relaxation Rates With Tumor Stage, Tumor Size, and Collagen Content

A logistic regression was performed to test if the T1 relaxation rate may be used to predict high-grade tumors (T3 or T4; refer to Fig. 6 for the corresponding graph). Although T1 relaxation time is a statistically significant predictor ($P < 0.01$), no exact prediction appears possible from the graph, as even with the highest T1 values the probability is not more than 75%, which seems clinically impractical to us, especially because it is, furthermore, not possible to distinguish between stages T1 and T2 or T3 and T4.

Regarding cRCC size and T1 relaxation rate, we found no correlation ($r = 0.02$; 95% CI, -0.34 to 0.37 ; $P > 0.05$). With reference to cRCC stage and the collagen content, we again obtained no significant association ($P > 0.05$). However, there was a trend for higher collagen

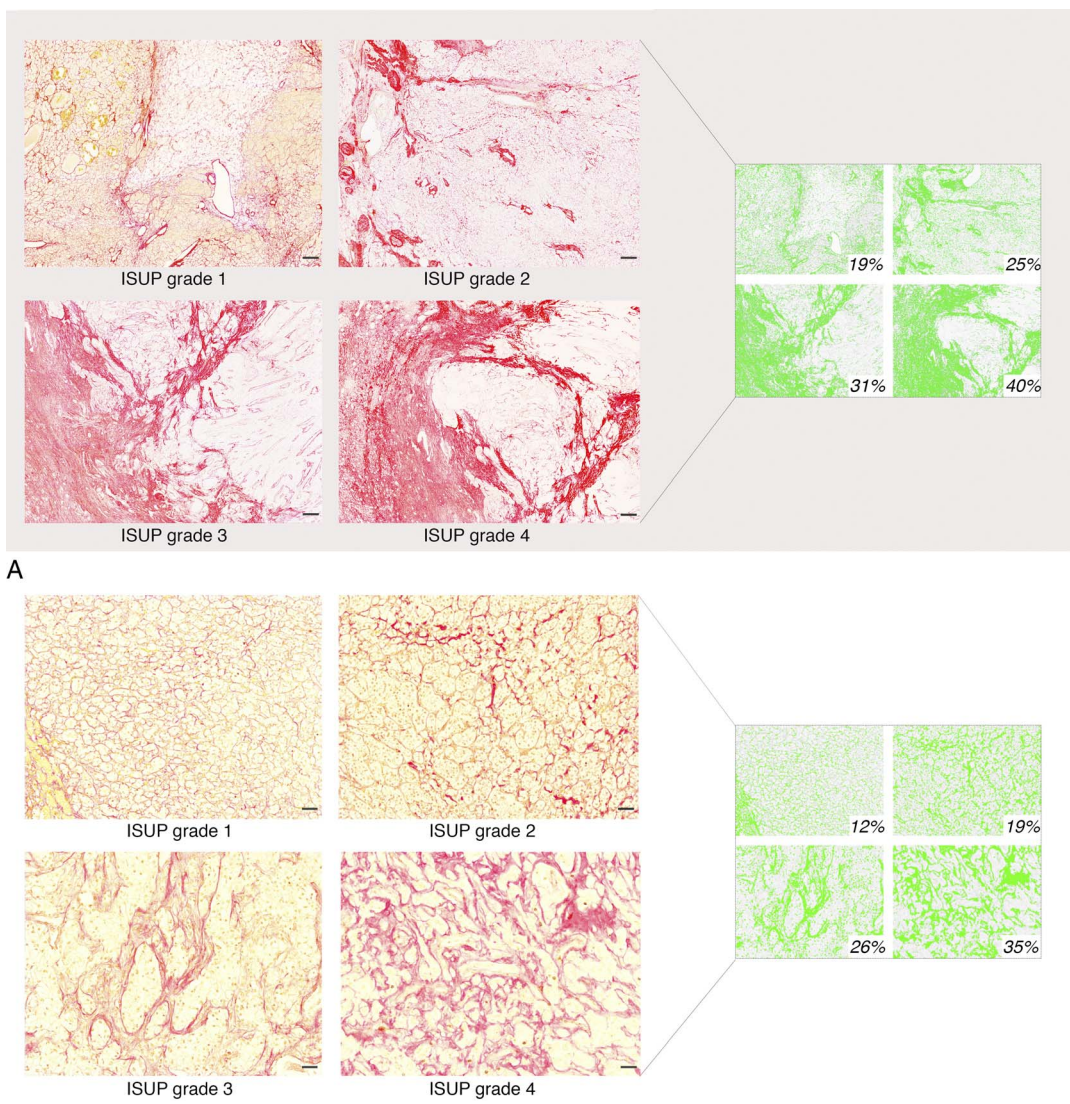


FIGURE 4. Measurement of histological collagen volume fraction. Examples of magnified ($\times 50/\times 100$) images in picrosirius red stained sections, (A) with 30 tiles and a bar indicating 500 μm and (B) with 2 tiles and a bar indicating 100 μm . Magnification images with 30 tiles were used for automated analysis with ImageJ to assess the collagen volume fraction (images on the right side of A). Examples demonstrated in this figure correspond to 19%, 25%, 31%, and 40% of collagen volume fraction for ISUP grades 1 to 4 for a periphery region and to 12%, 19%, 26%, and 35% for a central region of the tumor (with an exemplary 2 tiles for better visualization in higher magnified images).

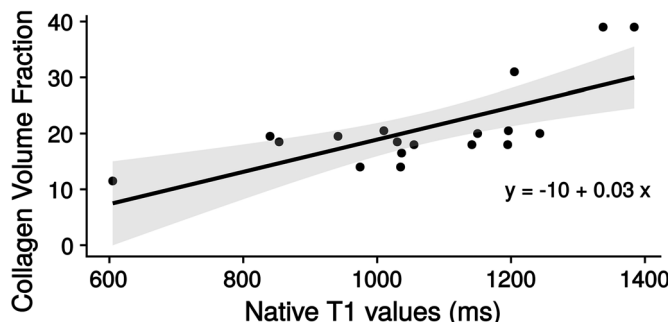


FIGURE 5. Association between native T1 values and the collagen volume fraction. Sections were stained with picrosirius red, and the collagen volume fraction was calculated as percentage of the collagen area, divided by the total depicted cRCC area. Native T1 values showed a strong correlation with the histological collagen volume fraction (correlation coefficient = 0.71), with the gray-colored area indicating confidence intervals.

content in higher tumor stages (refer to Supplementary Fig. S3, Supplemental Digital Content 3, <http://links.lww.com/RLI/A404>).

Interobserver Agreement for Quantitative T1 Measurements

Native cortical and medullary T1 values for both the cRCC group and the healthy cohort showed a convincing interobserver agreement. Specifically, for the cRCC group, mean ratios were 1.01 (95% CI, 0.96–1.05) for cRCC T1, 1.0 (95% CI, 0.96–1.04) for cortical T1, and 1.01 (95% CI, 0.93–1.09) for the medullary T1 relaxation time (refer to Fig. 7). Correspondingly, there was an excellent interobserver agreement for the healthy cohort, with an ICC of 0.99 for the cortex (95% CI, 0.96–1.00) and of 1.01 for the medulla (95% CI, 0.93–1.09). There was no significant difference of the average native cortical and medullary T1 relaxation times between the cRCC (cortex, 1035.0 ± 76.8 milliseconds; medulla, 1247.4 ± 73.2 milliseconds) and the healthy cohort (cortex, 1022.6 ± 55.0 milliseconds; medulla, 1255.7 ± 78.0 milliseconds; $P > 0.05$) (cRCC and healthy cohort: cortex, 1026.8 ± 65.6 milliseconds; medulla, 1254.8 ± 81.9 milliseconds).

DISCUSSION

The present study provides first time evidence that MRI-based native T1 mapping might allow a noninvasive evaluation and stratification of cRCC, correlating well with the collagen volume fraction measured in the histological samples. Higher native T1 values identified patients with higher ISUP grades. The clinical applicability of this approach is supported by the high interobserver agreement for the native cRCC and renal parenchyma T1 values. Native T1 mapping could, therefore, represent an *in vivo* biomarker for the differentiation of lower- and higher-grade cRCC, providing incremental diagnostic value beyond qualitative MRI features.

The main disadvantage of currently used MR SI measurements is that they are performed on qualitative nonparametric MR sequences, only allowing for semiquantitative/qualitative analysis, and that they depend on technical factors inherent to the MR signal acquisition, including choice of coil, slice thickness, and repetition time. By contrast, T1 longitudinal relaxation time is an intrinsic and fundamental tissue property, reflecting extracellular expansion and underlying pathophysiological processes and enabling a direct T1 quantification.¹⁶ The development of the MOLLI pulse sequence allowed the assessment of T1 relaxation times in a single breath-hold.¹⁷ So far, T1 mapping has mainly been used in the context of cardiovascular imaging, where mapping techniques have developed into an important clinical tool and were introduced into the clinical guidelines.¹⁸ In recent studies, the use of T1

mapping was extended beyond cardiovascular imaging into other body areas, including de novo approaches for assessment of hepatocellular carcinoma¹⁹ and renal corticomедullary differentiation in patients after kidney or lung transplantation.^{20,21}

Diffusion-weighted imaging (DWI) represents another MRI technique allowing for quantitative tissue characterization. Different from T1 mapping, it is based on the restriction of the random diffusion of water molecules within tissues, with the apparent diffusion coefficient (ADC) being calculated through linear regression from images taken at various b-values. The b-value reflects the strength and time spacing of the gradients used for the generation of DWI images. Previous studies have highlighted the potential of DWI to distinguish between malignant and benign lesions.^{22,23} With regard to DWI of RCC, there is a wide range of reported ADC values, whereby this may reflect the application of different MR scanners and sequence parameters.²⁴ It was indicated that RCC displayed lower ADC values compared with benign tissue.^{22,25} Some authors also proposed that DWI might be helpful to assess cRCC grade, such as the Gleason score in prostate carcinoma, but while the Gleason score is mainly related to cellularity, correlation with Fuhrman or ISUP grading requires additional reflection of tissue properties,²⁴ for which T1 mapping might be more advantageous. However, to date, there is limited research on the diagnostic comparison of DWI and T1 mapping generally and in particular with regard to kidney imaging, adding to the importance of future studies in this area. A previous study on renal fibrosis assessment in an animal model found that T1 mapping showed a better correlation with renal fibrosis than DWI, whereas another study suggested that DWI had a higher diagnostic performance.^{11,12} Both studies showed renal fibrosis to correlate with higher T1 relaxation times and lower ADC values.

Accounting for more than 80% of primary renal malignancies, cRCC is the most common subtype, often showing an aggressive

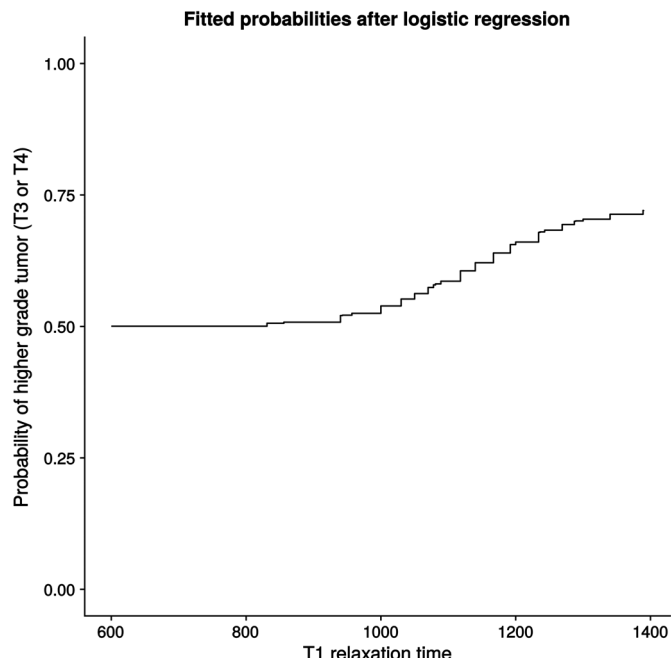


FIGURE 6. Association between T1 relaxation time and tumor stage. A logistic regression was performed, using T1 relaxation times to predict higher-grade tumors (T3 or T4 stage). Although T1 relaxation time was a statistically significant predictor ($P < 0.01$), no exact prediction appears possible from the graph. At low values, the probability of a high-grade tumor is 50%; at values above 1000, the probability increases. But even for the highest values, the probability does not increase above 75%.

behavior with a relatively high incidence of metastases and poorer survival rates compared with papillary and chromophobe RCC.^{26,27} Evaluation of tumor grade is of clinical relevance for prognosis and high-risk assessment for clear cell and papillary cRCC, being one of

the most powerful indicators for the prediction of biological aggressiveness, survival, and metastatic potential,^{24,28} with patients with higher-grade cRCC having a 4-fold higher risk for metastases compared with lower-grade cRCC patients and other RCC subtypes.²⁹ Both the

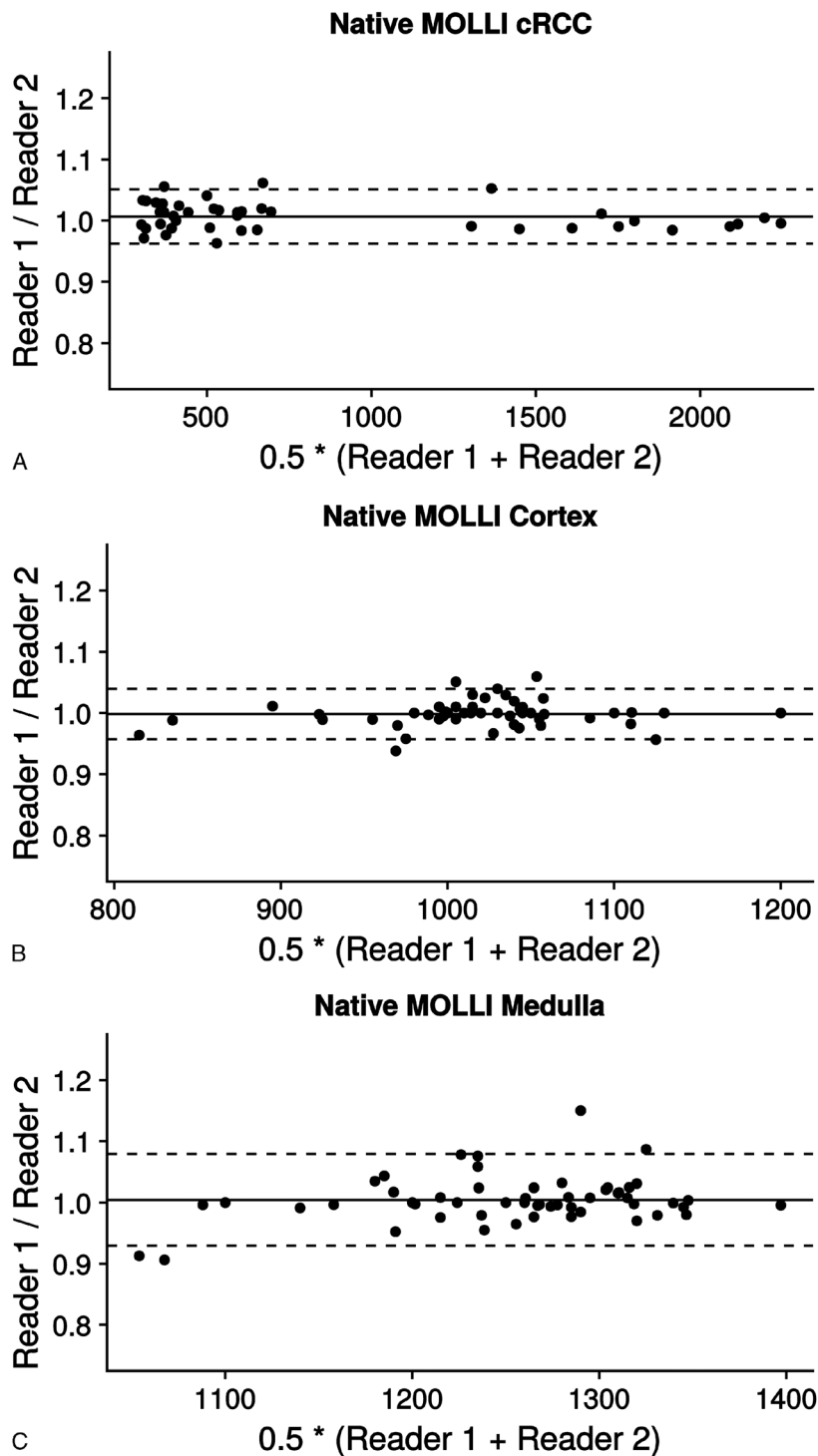


FIGURE 7. Interobserver agreement for native T1 values in the kidney cortex and medulla as well as in the tumor area. Bland-Altman plots illustrate the interobserver variability for RCC-related (A), cortical (B), and medullary (C) T1 values. Specifically, the mean ratios were 1.01 (95% CI, 0.96–1.05) for the cRCC T1, 1 (95% CI, 0.96–1.04) for cortical T1, and 1 (95% CI, 0.93–1.08) for the medullary T1 relaxation time. The mean ratio of the data is illustrated by the central horizontal line. The upper and lower reference lines indicate the upper and lower limits of agreement (96% confidence intervals).

increasing detection rate for small renal masses and a paradigm shift toward less invasive treatment options support the need for noninvasive tools to assess the grade and subtype of newly diagnosed renal masses, especially in patients with comorbidities. The possibility to predict nucleolar grade and stage preoperatively may improve prognosis assessment, prior patient information, and preoperative planning (partial nephrectomy/radical nephrectomy). In addition, it might prevent cases of upstaging after partial nephrectomy in larger tumors and help to identify patients eligible for immunotherapy with checkpoint inhibitors.³⁰ Generally, it could aid the selection of patients suitable for less invasive forms of therapy, such as thermal ablation or even active surveillance.⁸ Image-based grading could be particularly helpful and potentially cost-effective in patients with small renal masses with a higher probability of nondiagnostic biopsy or in patients with high comorbidities and higher risk for interventional procedures.³¹ The approach of the present study would be easy to translate into clinical practice due to absence of complex mathematic modeling and already existing commercial availability, with the option to acquire T1 maps automatically during the MRI scan.

Higher ISUP grade tumors are defined by higher nucleolar polymorphism and sarcomatoid or rhabdoid differentiation for grade 4 tumors.³² Sarcomatoid dedifferentiation with increasing ISUP grade, especially grade 4, results in an increase of the ECM. This is supported by a study by Delahunt et al,³³ who found evidence of abnormal collagen synthesis and assembly of a variety of collagen types in RCC with sarcomatoid transformation. In this sense, it seems reasonable that differences in the ECM between lower- and higher-grade cRCC may influence the specific T1 mapping values. Furthermore, T1 maps must be considered as complex variables, reflecting tissue properties besides the ECM. So, in addition, it may be that quantitative T1 values are also influenced by nucleolar differences between lower-grade and higher-grade cRCC. The abundance of ECM proteins such as collagen was shown to correlate well with native T1 values.³⁴ In this context, recent studies reported an association between the upregulation of ECM proteins and metastases and between the upregulation of collagen, for example, the collagen XXIII or VI α 1 chains, and tumor progression/poor prognosis in cRCC.^{2,4,35} Regarding histology, cRCC consists of cells with clear cytoplasm and necrosis; hemorrhage or cystic degeneration may occur.³⁶ In higher-grade cRCC, angiogenesis increases and causes higher degrees of cellularity and micronecrosis.³⁷ Tumor necrosis is present in up to 66% of cRCC and cannot only occur in the form of macroscopic zones, but also in form of micronecrosis as small microscopic regions below the spatial resolution of MRI, and might thus be included in the ROI analysis, possibly affecting native T1 times.^{6,30,38} In lower-grade cRCC, presence of cystic components (simple cysts as opposed to cystic degeneration with necrosis in higher-grade cRCC) may increase native T1 times and thus make the differentiation from higher-grade cRCC more challenging.

Apart from image-based grading, an image-based identification of different subtypes such as urothelial carcinoma, oncocytomas, chromophobe RCC, or lipid poor angiomyolipomas would be of interest as well, as it could potentially reduce the number of unnecessary surgical resections, considering that preoperative renal mass biopsy is still debated due to the risk of nondiagnostic biopsies and potential procedural complications.^{9,39} However, in the present study, the number of subtypes other than cRCC was too small to allow for any valid assessment ($n = 4$, with 2 oncocytomas and 2 urothelial carcinomas). For a comprehensive preoperative noninvasive assessment of tumor aggressiveness, further studies on T1 mapping are warranted, focusing on the ability to predict tumor grade as well as subtype.

For the present study, the quantitative T1 values obtained for the cortex and medulla were compared with those reported in the literature, whereby the mean and SD of the cortical T1 values in the native group of 1026.8 ± 65.6 milliseconds showed a good correlation with the value of 1082 ± 138 reported by Lee et al.⁴⁰ Prior research on cardiovascular

imaging suggested native T1 mapping as a reliable determinant of myocardial edema or fibrosis,⁴¹ showing a similar performance to native and contrast-enhanced T1 mapping in the detection and quantification of histological collagen volume fraction.⁴² Native imaging of the cRCC is advantageous, because (1) a substantial proportion of patients with cRCC are affected by renal impairment⁴³ and (2) recent findings indicated that gadolinium may accumulate in the central nervous system and other body tissues after repeated administration with unknown clinical significance.

An important limitation of the present study is its single-center design and the small number of patients, especially regarding higher-grade cRCC ($n = 10$), which is accompanied by a larger margin of error, although it is slightly strengthened by the performance of repeated measurements in the same subject by different observers. Also, there was size heterogeneity between the grades, especially between lower-grade (ISUP grades 1 and 2) and higher-grade (ISUP grades 3 and 4). This variation in size can be explained by the higher biological aggressiveness and rapid growth kinetics of higher-grade cRCC, which are thus more likely to be larger at diagnosis. Furthermore, although this study correlated different cRCC grades with histological collagen volume fraction in cRCC samples, the tissue samples only represented relatively small tumor sections, which cannot be accurately located based on MRI, because of which a sampling bias cannot be fully excluded. However, this technique is more accurate than biopsies, which are often performed for the validation of cardiovascular T1 mapping. In addition, the exclusion of other subtypes of renal masses carries the risk of potential selection bias. Besides, although larger areas of necrosis were excluded, smaller necrotic regions may have been included in the ROI areas and affected T1 measurements. Finally, imaging was performed with a single scanner and T1 mapping sequence, and reproducibility across different scanners and field strengths was not tested. Therefore, results may not be generalizable.

In conclusion, native T1 mapping may represent an *in vivo* biomarker for the differentiation of lower- and higher-grade cRCCs, providing incremental diagnostic value beyond qualitative MRI features, without the use of contrast agents. Native T1 values were significantly higher in patients with higher-grade cRCC, showing a strong correlation with the collagen volume fraction. The possibility of *in vivo* characterization using native T1 values has potential to optimize individualized treatment options, assisting in the selection of less invasive therapeutic options.

ACKNOWLEDGMENTS

L.C.A. and B.R. are grateful for her participation in the BIH Charité–Junior Clinician Scientist Program funded by the Charité–Universitätsmedizin Berlin and the Berlin Institute of Health. J.B. is a participant in the BIH–Twinning Grant Program funded by the Charité–Universitätsmedizin Berlin and the Berlin Institute of Health. M.R.M. is funded by the Deutsche Forschungsgemeinschaft (DFG, German Research Foundation) – SFB 1340/1 2018, 5943/31/41.

REFERENCES

1. Siegel RL, Miller KD, Jemal A. Cancer statistics, 2018. *CA Cancer J Clin.* 2018; 68:7–30.
2. Xu F, Chang K, Ma J, et al. The oncogenic role of COL23A1 in clear cell renal cell carcinoma. *Sci Rep.* 2017;7:9846.
3. Sherman-Baust CA, Weeraratna AT, Rangel LB, et al. Remodeling of the extracellular matrix through overexpression of collagen VI contributes to cisplatin resistance in ovarian cancer cells. *Cancer Cell.* 2003;3:377–386.
4. Wan F, Wang H, Shen Y, et al. Upregulation of COL6A1 is predictive of poor prognosis in clear cell renal cell carcinoma patients. *Oncotarget.* 2015;6:27378–27387.
5. Sengupta S, Lohse CM, Leibovich BC, et al. Histologic coagulative tumor necrosis as a prognostic indicator of renal cell carcinoma aggressiveness. *Cancer.* 2005; 104:511–520.

6. Delahunt B, McKenney JK, Lohse CM, et al. A novel grading system for clear cell renal cell carcinoma incorporating tumor necrosis. *Am J Surg Pathol.* 2013;37:311–322.
7. Karlo CA, Di Paolo PL, Chaim J, et al. Radiogenomics of clear cell renal cell carcinoma: associations between CT imaging features and mutations. *Radiology.* 2014;270:464–471.
8. Campbell S, Uzzo RG, Allaf ME, et al. Renal mass and localized renal cancer: AUU guideline. *J Urol.* 2017;198:520–529.
9. Leveridge MJ, Finelli A, Kachura JR, et al. Outcomes of small renal mass needle core biopsy, nondiagnostic percutaneous biopsy, and the role of repeat biopsy. *Eur Urol.* 2011;60:578–584.
10. Taylor AJ, Salermo M, Dharmakumar R, et al. T1 mapping: basic techniques and clinical applications. *JACC Cardiovasc Imaging.* 2016;9:67–81.
11. Child N, Suna G, Dabir D, et al. Comparison of MOLLI, shMOLLI, and SASHA in discrimination between health and disease and relationship with histologically derived collagen volume fraction. *Eur Heart J Cardiovasc Imaging.* 2018;19:768–776.
12. Sibley CT, Noureldin RA, Gai N, et al. T1 Mapping in cardiomyopathy at cardiac MR: comparison with endomyocardial biopsy. *Radiology.* 2012;265:724–732.
13. Woo S, Suh CH, Kim SY, et al. Diagnostic performance of DWI for differentiating high- from low-grade clear cell renal cell carcinoma: a systematic review and meta-analysis. *AJR Am J Roentgenol.* 2017;209:W374–W381.
14. Pallwein-Prettner L, Flory D, Rotter CR, et al. Assessment and characterisation of common renal masses with CT and MRI. *Insights Imaging.* 2011;2:543–556.
15. Moch H. The WHO/ISUP grading system for renal carcinoma. *Pathologe.* 2016;37:355–360.
16. Haaf P, Garg P, Messroghli DR, et al. Cardiac T1 Mapping and Extracellular Volume (ECV) in clinical practice: a comprehensive review. *J Cardiovasc Magn Reson.* 2016;18:89.
17. Look DC, Locker DR. Time saving in measurement of NMR and EPR relaxation times. *Rev Sci Inst.* 1970;41:250–251.
18. Messroghli DR, Moon JC, Ferreira VM, et al. Clinical recommendations for cardiovascular magnetic resonance mapping of T1, T2, T2* and extracellular volume: a consensus statement by the Society for Cardiovascular Magnetic Resonance (SCMR) endorsed by the European Association for Cardiovascular Imaging (EACVI). *J Cardiovasc Magn Reson.* 2017;19:75.
19. Peng Z, Li C, Chan T, et al. Quantitative evaluation of Gd-EOB-DTPA uptake in focal liver lesions by using T1 mapping: differences between hepatocellular carcinoma, hepatic focal nodular hyperplasia and cavernous hemangioma. *Oncotarget.* 2017;8:65435–65444.
20. Huang Y, Sadowski EA, Artz NS, et al. Measurement and comparison of T1 relaxation times in native and transplanted kidney cortex and medulla. *J Magn Reson Imaging.* 2011;33:1241–1247.
21. Peperhove M, Vo Chieu VD, Jang MS, et al. Assessment of acute kidney injury with T1 mapping MRI following solid organ transplantation. *Eur Radiol.* 2018;28:44–50.
22. Lassel EA, Rao R, Schwenke C, et al. Diffusion-weighted imaging of focal renal lesions: a meta-analysis. *Eur Radiol.* 2014;24:241–249.
23. Baltzer PAT, Bickel H, Spick C, et al. Potential of noncontrast magnetic resonance imaging with diffusion-weighted imaging in characterization of breast lesions: intraindividual comparison with dynamic contrast-enhanced magnetic resonance imaging. *Invest Radiol.* 2018;53:229–235.
24. Rosenkrantz AB, Niver BE, Fitzgerald EF, et al. Utility of the apparent diffusion coefficient for distinguishing clear cell renal cell carcinoma of low and high nuclear grade. *AJR Am J Roentgenol.* 2010;195:W344–W351.
25. Lopez Vendrami C, Parada Villavicencio C, DeJulio TJ, et al. Differentiation of solid renal tumors with multiparametric MR imaging. *Radiographics.* 2017;37:2026–2042.
26. Cheville JC, Lohse CM, Zincke H, et al. Comparisons of outcome and prognostic features among histologic subtypes of renal cell carcinoma. *Am J Surg Pathol.* 2003;27:612–624.
27. Mikami S, Oya M, Mizuno R, et al. Invasion and metastasis of renal cell carcinoma. *Med Mol Morphol.* 2014;47:63–67.
28. Novara G, Martignoni G, Artibani W, et al. Grading systems in renal cell carcinoma. *J Urol.* 2007;177:430–436.
29. Guethmundsson E, Hellborg H, Lundstam S, et al. Metastatic potential in renal cell carcinomas <=7 cm: Swedish Kidney Cancer Quality Register data. *Eur Urol.* 2011;60:975–982.
30. Powles T, Albiges L, Staehler M, et al. Updated European Association of Urology Guidelines Recommendations for the Treatment of First-line Metastatic Clear Cell Renal Cancer. *Eur Urol.* 2017;S0302-2838:31001–31001.
31. Cornelis F, Tricaud E, Lasserre AS, et al. Multiparametric magnetic resonance imaging for the differentiation of low and high grade clear cell renal carcinoma. *Eur Radiol.* 2015;25:24–31.
32. Dagher J, Delahunt B, Rioux-Leclercq N, et al. Clear cell renal cell carcinoma: validation of World Health Organization/International Society of Urological Pathology grading. *Histopathology.* 2017;71:918–925.
33. Delahunt B, Bethwaite PB, McCredie MR, et al. The evolution of collagen expression in sarcomatoid renal cell carcinoma. *Hum Pathol.* 2007;38:1372–1377.
34. Robbers LF, Baars EN, Brouwer WP, et al. T1 mapping shows increased extracellular matrix size in the myocardium due to amyloid depositions. *Circ Cardiovasc Imaging.* 2012;5:423–426.
35. Ho TH, Serie DJ, Parasramka M, et al. Differential gene expression profiling of matched primary renal cell carcinoma and metastases reveals upregulation of extracellular matrix genes. *Ann Oncol.* 2017;28:604–610.
36. Campbell N, Rosenkrantz AB, Pedrosa I. MRI phenotype in renal cancer: is it clinically relevant? *Top Magn Reson Imaging.* 2014;23:95–115.
37. Pedrosa I, Alsop DC, Rofsky NM. Magnetic resonance imaging as a biomarker in renal cell carcinoma. *Cancer.* 2009;115(suppl 10):2334–2345.
38. Klatte T, Said JW, de Martino M, et al. Presence of tumor necrosis is not a significant predictor of survival in clear cell renal cell carcinoma: higher prognostic accuracy of extent based rather than presence/absence classification. *J Urol.* 2009;181:1558–1564; discussion 63–64.
39. Prezzi D, Neji R, Kelly-Morland C, et al. Characterization of small renal tumors with magnetic resonance elastography: a feasibility study. *Invest Radiol.* 2018;53:344–351.
40. Lee VS, Kaur M, Bokacheva L, et al. What causes diminished corticomедullary differentiation in renal insufficiency? *J Magn Reson Imaging.* 2007;25:790–795.
41. Germain P, El Ghannudi S, Jeung MY, et al. Native T1 mapping of the heart—a pictorial review. *Clin Med Insights Cardiol.* 2014;8(suppl 4):1–11.
42. Nakamori S, Dohi K, Ishida M, et al. Native T1 mapping and extracellular volume mapping for the assessment of diffuse myocardial fibrosis in dilated cardiomyopathy. *JACC Cardiovasc Imaging.* 2018;11:48–59.
43. Russo P. End stage and chronic kidney disease: associations with renal cancer. *Front Oncol.* 2012;2:28.